MASTER OF SCIENCE DISSERTATION

Dissecting the contribution of dendritic computations in Fast Spiking Interneurons synaptic integration.

Author: Alexandra I. Tzilivaki

Post graduate program in Molecular biology and Biomedicine

University of Crete

Faculty of Health, Medical School

Faculty of Natural Sciences, Department of Biology

Foundation for Research and Technology Hellas

Institute of Molecular Biology and Biotechnology

To my family

To Spinal Muscular Atrophy patients

To people who truly love Brain Research

Δόξα τω Θεώ!

This research work was supported by Google with the Google Europe Scholarship

By the Alexander C. Onassis Benefit Foundation Scholarship

By IMBB FORTH Scholarship.

ACKNOWLDGMENTS

ABSTRACT

Interneurons are critical for the proper functioning of neural circuits and are typically considered to act as linear point neurons. However, exciting new findings reveal complex, sub- and/or supralinear computations in the dendrites of various interneuron types. These findings challenge the point neuron dogma and call for a new theory of interneuron arithmetic. Using detailed, biophysically constrained models, we predict that dendrites of FS basket cells in both the hippocampus and mPFC come in two flavors: supralinear, supporting local sodium spikes within large-volume branches and sublinear, in small-volume branches. Synaptic activation of varying sets of these dendrites leads to somatic firing variability that cannot be explained by the point neuron reduction. Instead, a 2-stage Artificial Neural Network (ANN), with both sub- and supralinear hidden nodes, captures the variance. We propose that FS basket cells have substantially expanded computational capabilities sub-served by their non-linear dendrites and act as a 2-layer ANN.

Contents

1 INTRODUCTION

1.1 Brain Anatomy and Function

1.1.1 The Hippocampus

The hippocampus, (also known as archicortex) is a critical structure of the mammalian brain. There are two hippocampi, one of each side of the brain. The hippocampus is located under the cerebral cortex and specifically the temporal lobe. It is a part of the limbic system and plays a significant role in memory formation, storage and consolidation[1] as well as in spatial navigation [2] and other executive functions. The hippocampus can be subdivided into 3 subregions; the hippocampus proper (consisting of four Cornu Ammonis areas – CA4, CA3, CA2 and CA1), the dentate gyrus and the subiculum. Hippocampus accompanying with presubuculum, parasubiculum and entorhinal cortex form a structure known as hippocampal formation [3]. The basic connectivity patterns among hippocampal neurons are conserved among all mammalian species.

1.1.2 The Prefrontal Cortex

The prefrontal cortex (PFC), is defined as the cortical region in the anterior frontal lobe of the mammalian brain. In particular, it is considered as the part of the cerebral cortex that receives projection fibers from the mediodorsal nucleus of the thalamus. The PFC lies in front of the premotor cortex and in the front lateral surface of the limbic association cortex on the orbital and medial surfaces[4]. In rodents, the average PFC is composed of five layers. The prefrontal cortex is devoted to the executive functions that control the goal-directed actions. It has actually been named the "executive center" of the brain. It is considered as the brain area that receives and integrates information and finally makes 'decisions'. Some of these "executive functions" that the PFC underlies are: Focusing attention, motor planning, thought organization, problem solving, predicting behavioral consequences, temporal organization, decision-making, behavioral inhibition, rule learning and long-term memory storage [5]. Most of the above higher order cognitive functions require proper functioning of the working memory system.

1.2 GABAergic interneurons

GABAergic interneurons play a key role in modulating neuronal activity and

transmission in multiple brain regions[6–10]. Among others, they are responsible for controlling the excitability of both excitatory and inhibitory cells, modulating synaptic plasticity and coordinating synchrony during neuronal oscillations[7,11–13,14]. GABAergic interneurons come in a variety of molecular profiles, anatomical features and electrophysiological properties[6,8,15,16]. Despite this variability, many interneuron types exhibit similar computations, the most common being a precise EPSP-spike coupling[7,17,18]. As they innervate a large number of cells near the site of action potential initiation[3,13], they are believed to generate a powerful widespread inhibition, also referred to as an inhibitory blanket[19].

1.2.1 Fast Spiking Basket Cells

Fast Spiking (FS) basket cells constitute one of the main types of hippocampal and neocortical interneurons.[11,19,20] They are distinguished from other subtypes by molecular markers –e.g. the expression of the Parvalbumin (PV) protein-, their anatomical features[21], synaptic connectivity patterns[19,22] and membrane mechanisms such as the presence of calcium permeable AMPA receptors[23,11,24] and the high density of potassium channels in their aspiny dendritic trees[10,20,25,26,11].

A growing body of literature recognizes the importance of FS basket cells in controlling executive functions such as working memory and attention as well as their role in neurodegenerative disorders[9,27,28]. However, little is known about the mechanistic underpinnings of FS basket cell contributions to these functions. Most studies have focused on the molecular and anatomical features of FS basket cells[12,18,21,25,29,30] and supported the dogma that these cells integrate inputs like linear –or at best sublinear- point neurons[31,32].

This dogma is based on the assumption that FS basket cells integrate synaptic inputs in a linear manner, completely ignoring potential dendritic infuences[11]. Active dendritic mechanisms however, are known to transform incoming information in non-trivial ways, thus greatly influencing output signals[33,34,35,36]. Despite its fundamental role in neuronal computations, dendritic integration has been studied mainly in excitatory pyramidal cells[33,37–44]. The current knowledge about FS basket cell dendrites entails a passive backpropagation of APs, low density of sodium channels[11] and high density of

fast, high-threshold potassium channels in distal dendrites[11,45,46]. All of the above contribute to sublinear dendritic integration, coupled to fast and temporally precise AP initiation in response to synaptic input[18,31], largely in line with the simplified point-neuron view of interneurons.

Exciting new findings however, reveal that the dendrites of certain interneuron types are much more powerful than originally assumed. For example, sublinear dendritic EPSP integration along with supralinear calcium accumulations has been reported in cerebellar Stellate Cells (SCs)[17,47].Moreover, RAD dendrite-targeting interneurons in the CA1 area exhibit calcium supralinearities[48] while in the CA3, both calcium nonlinearities and sodium spikes in FS basket cell dendrites during sharp wave ripples, have been reported[7]. The exact nature of dendritic computations in FS basket cells, however, is unknown. As a result, whether a linear point neuron or a more sophisticated abstraction -like the two-stage[38] or multi-stage integration[49] proposed for pyramidal neurons- can successfully capture their synaptic integration profile, remains an open question.

1.3 Motivation of the Study

To address this question, we developed detailed, biologically constrained biophysical models of FS basket cells using anatomical reconstructions of both hippocampal [50] and cortical (medial Prefrontal Cortex) neurons[51] (shown in figure 2). Synaptic stimulation within the dendrites of model cells predicts the co-existence of two distinct integration modes; some dendrites exhibit supralinear synaptic integration while others operate in a sublinear mode (figure 6, 7, 8). Morphological features such as dendritic length and/or diameter influence the integration mode and these features differ between hippocampal and cortical neurons. Interestingly, dendritic volume appears to be a consistent discriminating feature among sub- and supralinear dendrites of both areas (figure 11). By generating a large number of different spatial patterns of synaptic activation we find that spatially dispersed inputs lead to higher firing rates than inputs clustered within a few dendrites in both Hippocampus and PFC models (figure 12), opposite to respective simulations in pyramidal neurons[52]. Moreover, a 2-layer Artificial Neural Network

(ANN) with both sub- and supralinear hidden nodes can predict the firing rate of the aforementioned models much better than a linear ANN (figures 13-16, Table 7).

1.4 Impact of the study

This is the first study that provides a systematic, cross-area analysis of dendritic integration in FS basket cells. Our findings challenge the current dogma, whereby interneurons are treated as linear summing devices, essentially void of dendrites. We predict that the dendrites of FS basket cells in both Hippocampal and Neocortical regions can operate in distinct non-linear modes. As a result, FS basket cells, similar to pyramidal neurons[38], are better represented by a 2-stage integrator abstraction rather than a point neuron.

2 Methods

Simulations were performed on a High-Performance Computing Cluster equipped with 312 CPU cores and 1.150 Gigabytes of RAM, under 64-bit CentOS 6.7 Linux.

2.1 Compartmental modeling

All 8 model neurons were implemented within the NEURON simulation environment (version 7.3)[53]. Detailed morphological reconstructions of the 5 Fast spiking Basket cells of the rat Hippocampus were adopted from Tukker et al. 2013[50], via the NeuroMorpho.org database. Due to the lack of axonal reconstructions, we used the axon from the B13a.CNG.swc reconstruction for all 5 hippocampal neuron models. The 3 PFC morphologies were adopted from Rotaru et al. 2011[51], via the NeuroMorpho.org database and included their respective axons.

Dendritic branches with mean diameter values larger than 1.2 μm were excluded from all simulations and data analysis procedures, based on Emri et al. 2001[54]. The NLM Morphology Viewer Software was used to transform morphological reconstructions into .hoc files.

2.2 Biophysical Properties of FS Basket Cells Models

All model neurons were calibrated with respect to their biophysical properties so as to conform to experimental data. The same active and passive properties were used in all model cells, with the exception of very small modifications in the conductances of somatic/axonal Sodium and Kdr mechanisms (Tables 1 and 2). The latter were necessary to account for the influence of morphological variability on neuronal responses.

Conductances of all active ionic mechanisms were adapted from Konstantoudaki et al. 2014[55]. Both hippocampal and PFC models include fast voltage-dependent sodium channels (g_{nafin}), delay rectifier potassium channels (g_{kdrin}), slow inactivation potassium channels (g_{slowin}), slow calcium dependent potassium channels (g_{kcain}), A-type

potassium channels for proximal and distal dendritic regions (g_{kadin}, g_{kapin}), h currents (g_{hin}), and L-, N- and T- type voltage-activated calcium channels (g_{cal}, g_{can} and g_{cat}, respectively). Sodium current conductances were substantially larger in axonal compared to somatic compartments, which were in turn an order of magnitude larger than dendritic sodium conductances[11]. Moreover, dendritic branches located beyond 100 microns from the soma (distal dendrites) had smaller sodium conductances than proximal branches (located less than 100 microns from the soma) as per[11,46]. A calcium buffering mechanism was included in all compartments. Details about all biophysical mechanisms are listed in Table 2.

Table 1. Passive properties of biophysical models

	Soma	*Axon*	*Proximal dendrites*	*Distal Dendrites*
Leak conductance (*g_pas*)[18]	1.315e-4 S/cm^2	3.55e-6 S/cm^2	1.315e-4 S/cm^2	1.34e-5 S/cm^2
Resting Membrane Potential (e_pas)[18,25]	-68 mV	-68 mV	-68 mV	-68 mV
Membrane capacitance (*cm*) [18]	1.2 uf/cm^{-2}	1.2 uf/cm^{-2}	1.2 uf/cm^{-2}	1.2 uf/cm^{-2}
Axial Resistance (*Ra*) [18]	172 ohm/ cm	172 ohm/ cm	142 ohm/ cm	142 ohm/ cm

Table 1: Passive properties common to the 8 biophysical models

Table 2. Active properties of biophysical models				
Ion channel (S/cm^2)	*Soma*	*Axon*	*Proximal dendrites*	*Distal Dendrites*
Na_v [11,32,56]	0.145(PFC1-3) /0.396 (Hipp1-3) /0.828(Hipp4,5)	0.675(PFC1-3) /1.296(Hipp1-3) /1.512(PFC4,5)	0.018	0.014
H_v	0.00001	X	x	X
Kdr_v	0.036 (PFC)/ 0.0432(Hipp)	0.108 (PFC)/ 0.144 (Hipp)	0.0009	0.009
$Kslow_v$	0.000725	X	x	X
Kct_v	0.0001	X	x	X
Kca_v	0.02	X	x	X
Ka_v (proximal type) [56]	0.0032	X	0.001	0.0009
Ka_v (distal type) [57]	x	X	x	0.00216
Cal_v	x	X	0.00003	0.00003
Can_v	x	X	0.00003	0.00003
Cat_v	x	X	0.0002	0.0002
Calcium buffering dynamics	Yes	No	Yes	Yes

Table 2: Active membrane conductances across somatic, axonal, proximal (≤100 microns from the soma) and distal (>100 microns from the soma) dendritic compartments. Sodium current conductances are larger in axonal than somatic compartments. Dendritic sodium conductances are ~10 times smaller than axo-somatic conductances.

2.3 Synaptic conductances

Calcium permeable (GluR2-lacking) AMPA, NMDA and autaptic GABAa synaptic currents were incorporated in all model cells. Synaptic weights were validated so as to reproduce the current waveforms depicted in Wang Gao et al 2009[58] and Bacci et al 2003[25] and are shown in Table 3 and figure 5.

Table 3. Synaptic mechanisms of biophysical models	
Synaptic Current	Conductance Weight
Autaptic GABAa	71.1e-4
Ca permeable AMPA	7,5e-4
NMDA	16e-4

Table 3: Validated Synaptic conductance weight values of Autaptic GABAa Calcium permeable AMPA and NMDA currents, used in all simulations.

2.4 Electrophysiological validation

All model neurons were heavily validated against experimental data in order to ensure biological plausibility (figure1). Averaged electrophysiological values for the model cells and respective experimental values are shown in Table 4.

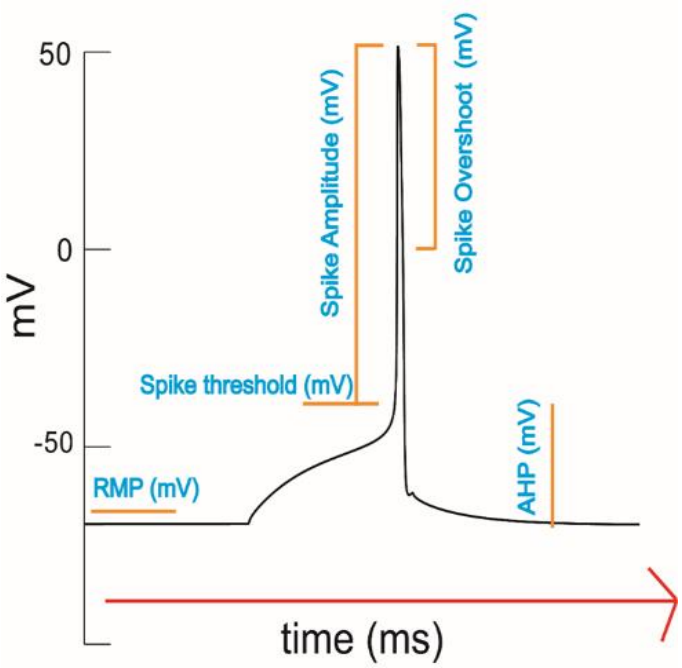

Figure 1: Action potential features of Fast Spiking Basket cells.

Table 4. Electrophysiological properties of biophysical models		
Value	*Model*	*Experimental data*
rHeobase *(pA)*[21]	150.0 ± 30.0	123 ± 58
Input Resistance (Ohm)[21]	97.7 ± 30.0	182 ± 83
Spike threshold (mV)[21]	-37.0 ± 3.0	-34 ± 2
Spike amplitude (mV)[21]	52.0 ± 2.0	53.0 ± 8.0
Spike half width (msec)[21],[25]	0.5 ± 0.1	0.2 ± 0.01/0.38 ± 0.008
f-i slope (Hz/pA)[25]	0.26 ± 0.03	0.2 ± 0.002
AHP (mV)[19]	24.6 ± 2.6	24.3 ± 0.7/23 ± 5

Table 4: Validation of electrophysiological properties.

2.5 Bi-modal dendritic integration in Fast Spiking Basket cells.

To map the dendritic integration profiles of our model neurons, we activated increasing numbers of synapses (1 to 20, with step 1) in each dendrite and recorded the voltage responses both locally and at the cell body for 100 ms. Synaptic input was simulated as a single depolarizing pulse, as per Poirazi et al 2003a[37]. Sodium conductances in somatic and axonal compartments were set to zero in order to avoid backpropagation effects. 12 autaptic events were also activated in somatic compartments[59].

2.5.1 Integration modes

Integration modes were deduced by comparing the measured dendritic/somatic responses (Actual maximum EPSP) against what would be expected if synaptic depolarizations summed linearly (Expected maximum EPSP). A dendrite was termed supralinear if Actual responses were larger than Expected, even if this was true only for a short range of synaptic inputs. A dendrite was considered sublinear if the Actual EPSPs were smaller than the Expected values for all synaptic inputs tested.

2.5.2 Sensitivity analysis

Sensitivity analysis was performed by modifying the conductances of NMDA, calcium-permeable AMPA receptors, Voltage gated Calcium Channels (VGCCs), Sodium, and A-type (proximal and distal) mechanisms by ± 20%. Increasing numbers of synapses (for 1 to 40) were used to assess possible changes in single branch integration. Results for all manipulations are shown in figure 10.

2.6 Morphological determinants of dendritic integration mode

Mean dendritic diameter and total dendritic length for supralinear and sublinear dendrites were measured for all reconstructed neurons. Dendritic volume was calculated according to the following formula:

$$V = \left(\pi * \left(\frac{diam}{2}\right)^2\right) * length \quad (\mu m^3)$$

Statistical analysis for all morphological features was performed using Student's t-test with equal sample sizes and assuming unequal variances (Welch's t-test).

2.6.1 Synaptic Stimulation Protocols

In all stimulation protocols, inputs were activated using a 50 Hz Poisson spike train. The maximum number of activated synapses was 60, as it was sufficient to induce firing at gamma related frequencies (30-100 Hz). The spatial arrangement of activated synapses was defined according to each of the following stimulation protocols:

2.6.2 Randomly dispersed, whole tree stimulation

Different numbers of synapses (N_{sysn} = 5, 10 up to 60) were randomly placed on randomly selected dendrites. For a given number of synapses N_{syn}, at each allocation step, one dendrite was chosen at random and one synapse was placed at a random location within this dendrite. For the selected dendrite, synaptic location was randomly changed 5 times. This process was repeated N times, where N was the number of dendrites for each model cell. This process ensured a realistic distribution of activated synapses within the entire dendritic tree of each modelled neuron.

2.6.3 Clustered, whole tree stimulation

The only difference of this protocol from the one described above is that each selected dendrite received a cluster (of size S_{clu} = 10 or 20) of synapses as opposed to a single synapse. For example, for N_{syn}=60 and Sclu = 10, a total of 6 dendrites were randomly selected to receive 10 synapses each. We followed the same experimental design as in the disperse, whole tree protocol. Thus, for a given number of synapses Nsyn, at each allocation step, one dendrite was chosen at random and one synapse was placed at a random location within this dendrite. For the selected dendrite, synaptic location was randomly changed 5 times. This process was repeated N times, where N was the number of dendrites for each model cell.

2.7 Artificial Neural Network Models

We constructed four feed-forward, backpropagation Artificial Neural Networks with

customized code written in MATLAB, version 2009: a) a 2-layer modular ANN whereby hidden neurons were divided in two parallel layers (1 & 2). In hidden layer 1, neurons consisted of supralinear (step-sigmoid) transfer functions while neurons in hidden layer 2 consisted of sublinear (saturating linear) transfer functions. The two types of transfer functions corresponded to respective supra- and sublinear dendrites of the biophysical model cells[60]. b) a 2-layer ANN with one hidden layer, whereby all hidden neurons had supralinear transfer functions, c) a 2-layer ANN with one hidden layer, whereby all hidden neurons had sub-linear transfer functions and d) a linear ANN whereby the hidden and output neurons had a linear transfer function (classical linear point neuron). In all ANNs, the output neuron had a linear transfer function. All ANNs were trained with the same input/output data sets and performance accuracy was estimated according to the correlation among predicted (by the ANN) and actual mean firing rates generated by the biophysical model, for a wide range of stimulation protocols. The parameters of each ANN are listed in **Table 5**. Firing rate corresponding to this particular configuration.

Table 5. ANN properties	
Train function	Levenberg-Marquardt backpropagation
Error Function	Mean squared normalized error performance
Number of epochs	1000
Type of network	feedforward

Table 5: Network parameters of all ANNs.

2.7.1 ANN training/testing datasets

Input to the four ANNs consisted of the number of synapses located in the modelled

dendritic branches and the target output consisted of the mean firing rate generated by the biophysical model in response to synaptic stimulation. In the biophysical model, these synapses were activated with the Dispersed and Clustered protocols described above as well as five new protocols using the same pattern of repetition trials as described above: 1) Randomly dispersed activation of synapses (Nsyn=2:2:60) in the entire dendritic trees. 2,3) Clustered (Sclu=3, Nsyn=20) or 4,5) Dispersed (Nsyn 10) synaptic allocation on supralinear dendrites and Clustered or Dispersed synaptic allocation on sublinear dendrites, respectively. Data shown in Figures 15, 16 correspond to PFC3 and HIPP2 model neurons and are representative of all model cells.

2.7.2 Linear Regression and Statistical Analysis.

We calculated the correlation coefficient (R) between Actual Mean Firing Rates (Target rates, in Hz) generated from the biophysical models and Predicted Mean Firing Rates (Predicted rates, in Hz) generated by the trained ANNs, respectively. Statistical analysis between Target and Predicted firing rates was performed using Student's t-test with equal sample sizes and assuming unequal variances (Welch's t-test).

3 RESULTS

3.1 The models

A total of 8 biophysical model neurons were built within the NEURON simulation environment[53]. We used realistic reconstructions of FS basket cells from the rat hippocampus (5 cells)[50] and from the mPFC (3 cells)[51] of mice (figure 2). All morphologies were downloaded from the Neuromorpho.org database and checked for reconstruction accuracy (diameter) (See Methods). To ensure biological relevance, ionic and synaptic conductances as well as basic membrane properties of model cells were heavily validated against experimental data[11,18,21,25,46,57] (see Tables 1-4 and figures 3-5). Moreover, for consistency reasons, the same set of biophysical mechanisms (type and distribution) was used in all model cells. This is to our knowledge the first set of detailed, biologically realistic models of FS basket cells from two brain areas.

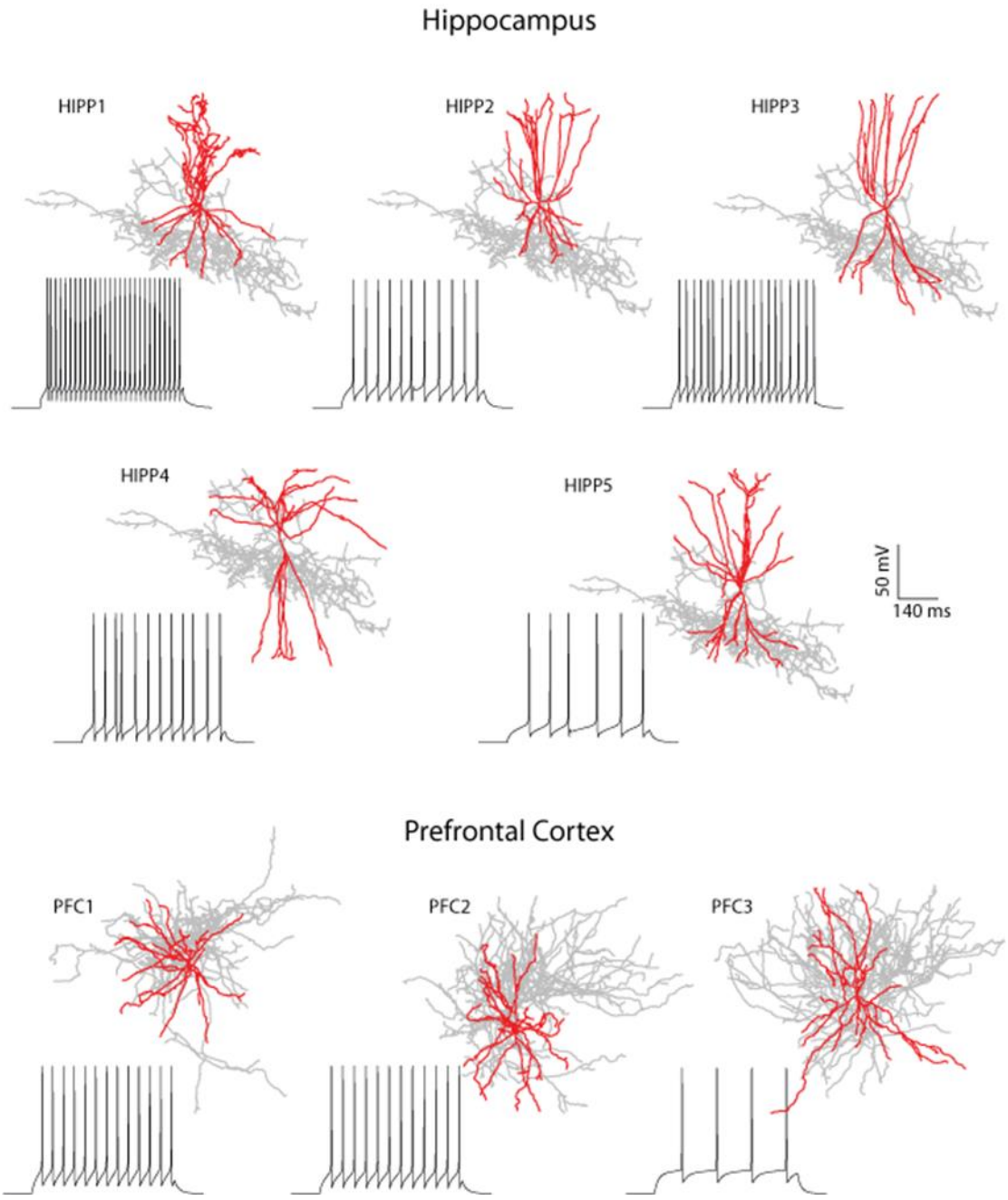

Figure 2:

Fast spiking basket cell reconstructions from 5 Hippocampal and 3 PFC interneurons. Dendrites are shown in red. Firing patterns in response to 200 pA current injection at the cell body are also shown for each morphology.

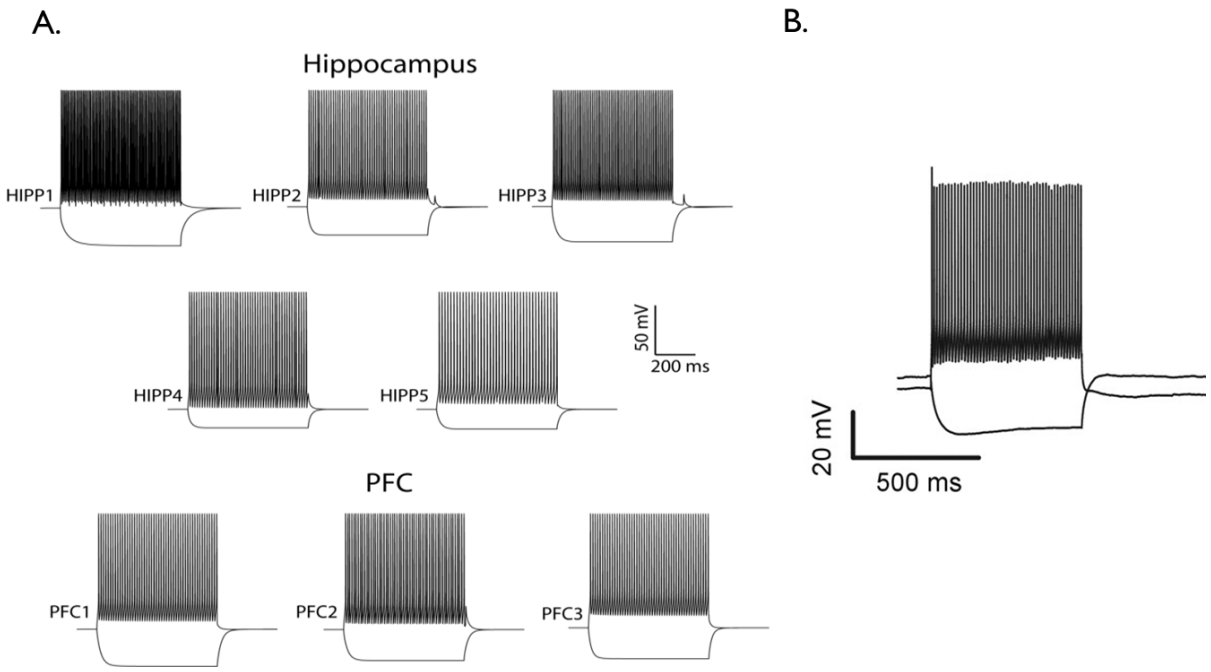

Figure 3.

Model cell firing profiles. Somatic Current-clamp traces of Hippocampal (A) and PFC (B) model cells, after a depolarizing current injection in somata (500 pA; 1000 ms) evoked a high-frequency firing pattern. A hyperpolarizing current injection in somata (-300pA, 1000ms) induced a realistic hyperpolarizing response.

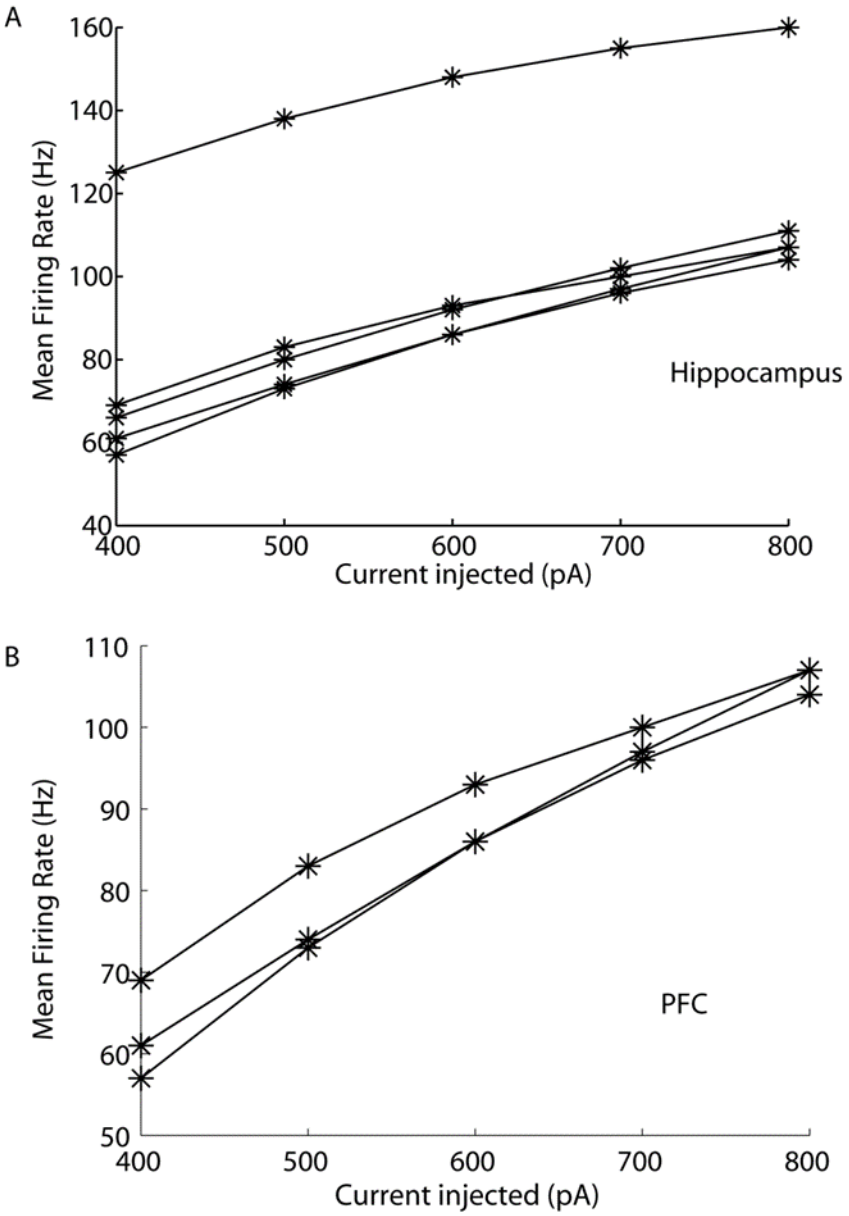

Figure 4:

Mean firing frequencies in response to injected currents of different amplitudes (600 ms duration) in Hippocampal (A) and PFC (B) model cells.

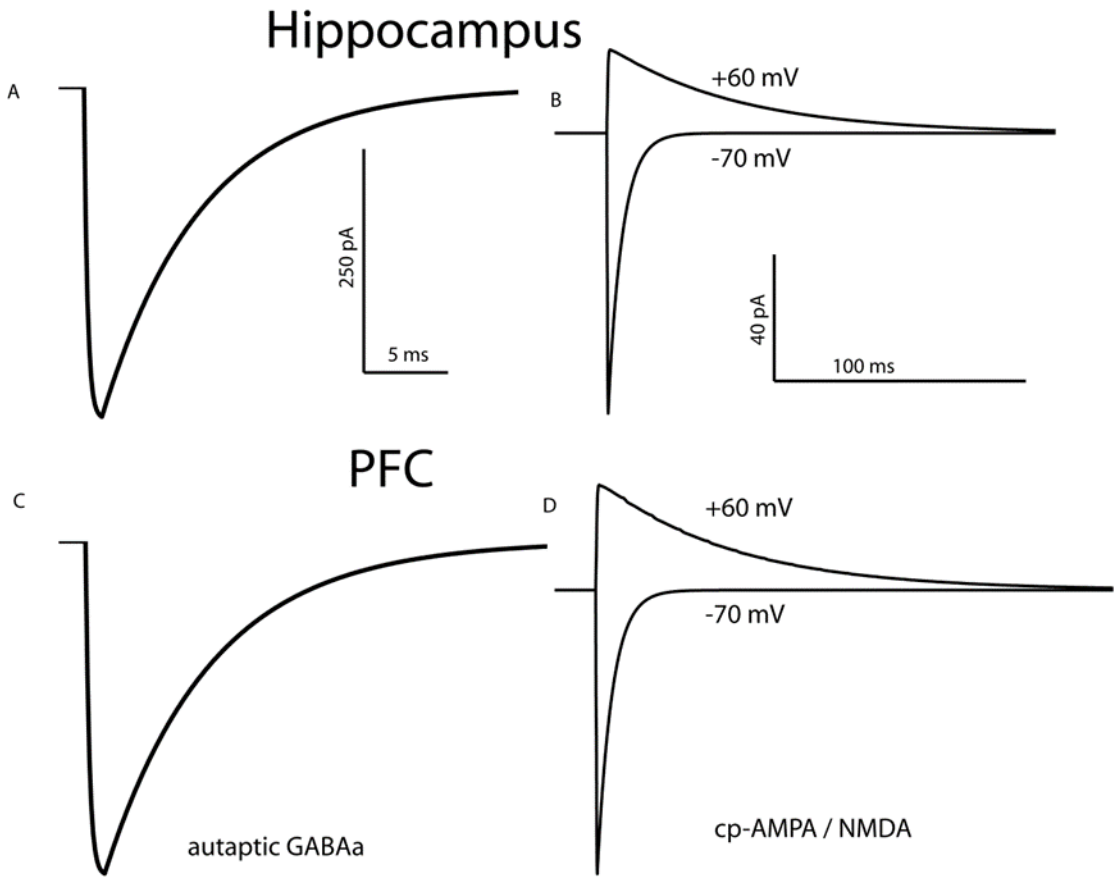

Figure 5: Validation of synaptic currents in Fast Spiking basket cells.

A,C: A three-step voltage clamp of voltage changes from −70 mV to 10 mV (duration 1 ms) and back to −70 mV was used to produce a self-inhibitory (autaptic) current. During the validation of this current, the reversal potential of Cl− was adjusted from −80 to −16 mV, in order to reproduce the experimental set up of Bacci et al., 2003[25]. However, a physiological reverse potential (−80 mV) was used for all other simulations. B,D: Model reproduction of cp-AMPA (−70 mV) and NMDA (+60 mV) currents in response to stimulation of 2 synapses as per Wang et al., 2009[58]. * Each trace represents the mean of all Hippocampal and PFC cells respectively.

3.2 Bi-modal dendritic integration in Fast Spiking Basket cells

The first step for deducing a realistic abstraction of FS basket cells is the systematic characterization of dendritic/neuronal integration properties across a significant number of neurons and dendrites. Towards this goal, we simulated gradually increasing excitatory synaptic input to the dendrites of all neuronal models (total of 637 simulated dendrites) and recorded the voltage response both locally (figure 6) and at the soma (figure 7)[17,37]. Increasing numbers of synapses (1:1:20) were uniformly distributed in each stimulated dendrite and activated synchronously with a single pulse. Sodium conductances in somatic and axonal compartments were set to zero, to avoid AP backpropagation contamination effects. We compared measured EPSPs to their linearly expected values, given by the number of activated inputs multiplied by the unitary EPSP. We found that within the same dendritic tree, branches summate inputs either in a supralinear or a sublinear mode (figures 6,7,8). While there were differences in the number of dendrites and proportions of sub- vs. supralinear dendrites, all of the morphologies tested expressed both integration modes (Table 6). Importantly, while both modes have been suggested in distinct interneuron types[17,48], this is the first study that predicts their co-existence within a single cell.

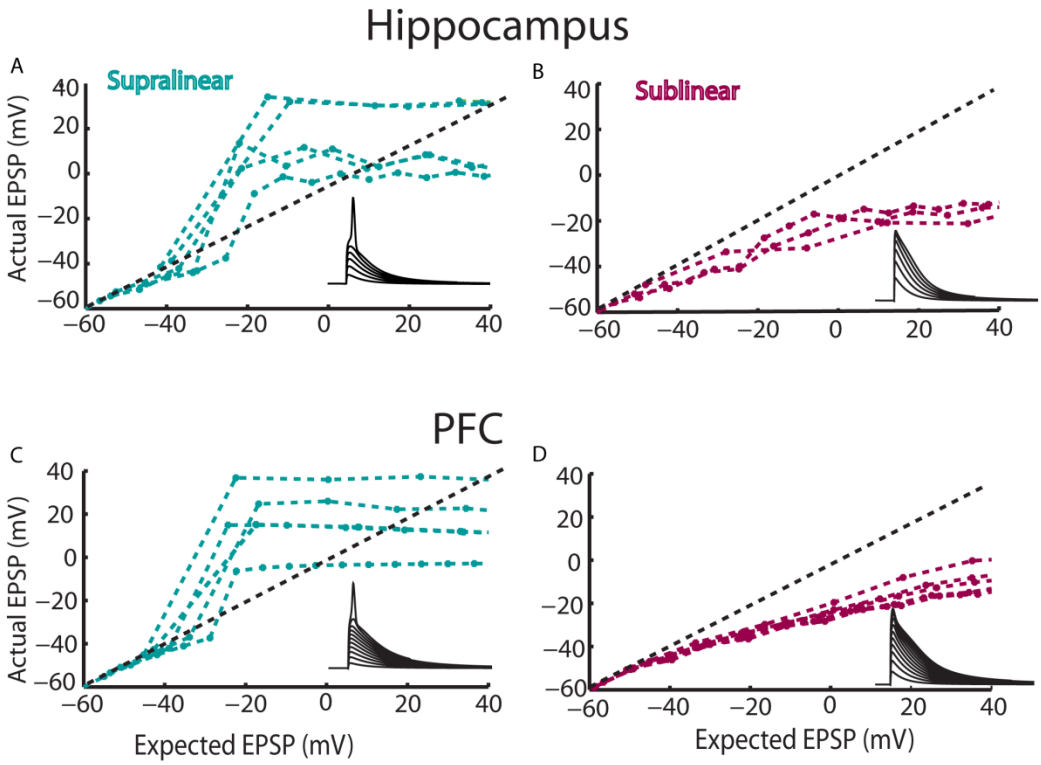

Figure 6:

Bimodal dendritic integration in FS basket cell models. Representative recordings from supralinear (A,C) and sublinear (B,D) dendritic branches in Hippocampal (top) and PFC (bottom) biophysical model interneurons, in response to synaptic stimulation. Increasing numbers of synapses (1:1:20) were uniformly distributed within each activated branch and activated with a single pulse. The y-axis shows the actual peak depolarization caused by synaptic activation while the x-axis shows the expected peak depolarization that would result from the linear summation of unitary EPSPs. The dashed line indicates linearity.

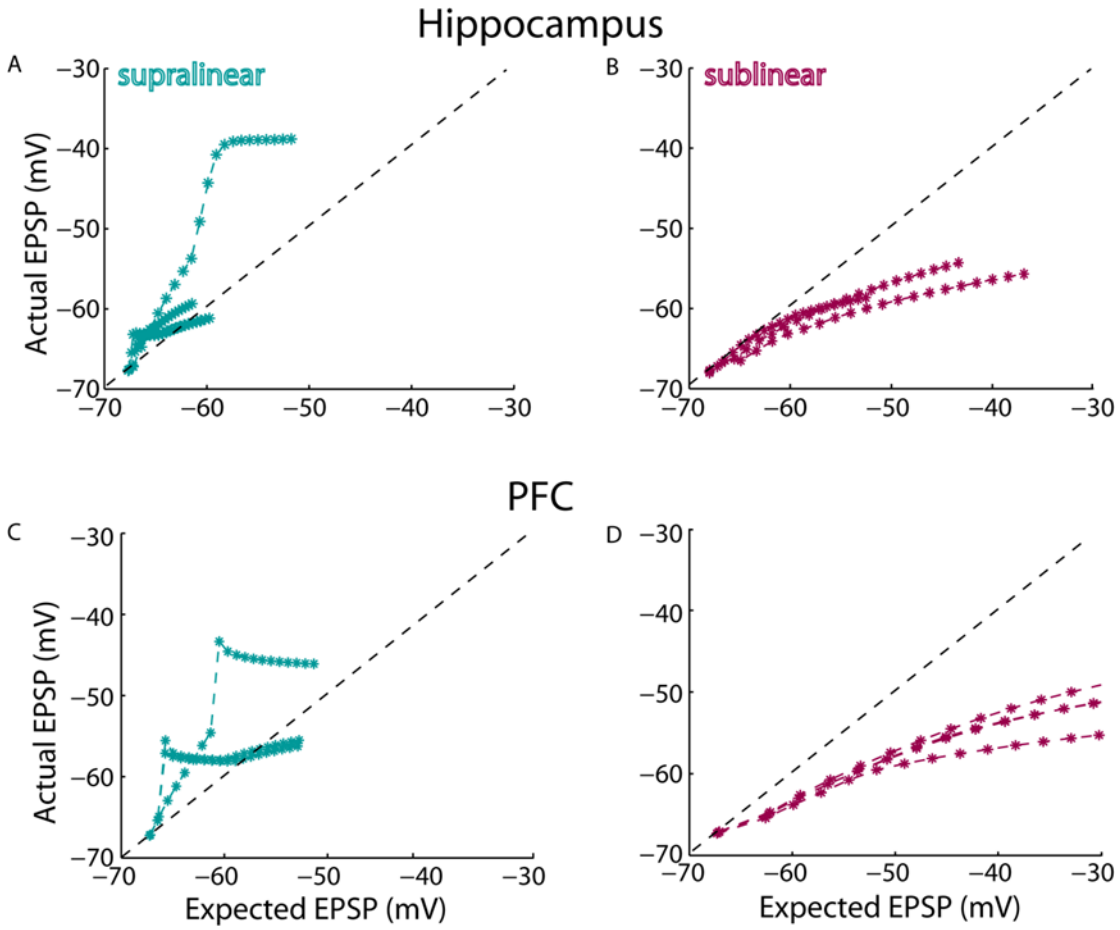

Figure 7:

Bimodal non-linear integration in Fast Spiking basket cells. Representative Somatic EPSPs after stimulation (single pulse) of an increasing number of synapses (1:1:20), uniformly distributed within dendrites.

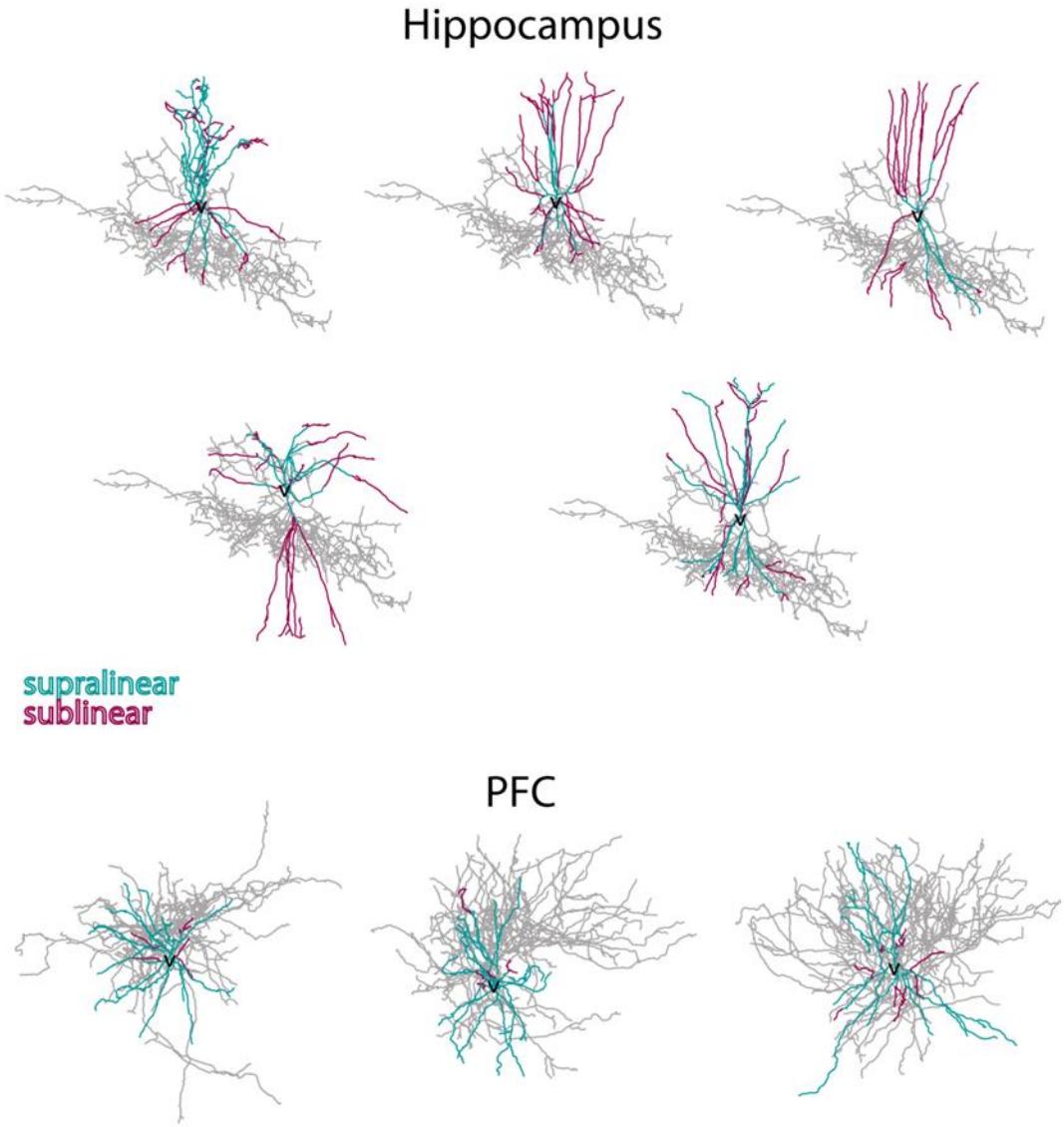

Figure 8:

Related to figure 2. Bimodal non-linear integration in Fast Spiking basket cells. Supralinear (blue) and sublinear (magenta) dendrites shown in each model cell.

Blocking sodium currents in dendrites totally eliminates supralinear EPSP responses (figure 9). To assess the robustness of this finding, we performed a sensitivity analysis whereby the cp-AMPA, NMDA, VGCCs, sodium and IA potassium conductances were

varied by ±20% of their control value. We found no changes in the integration mode of dendrites (data not shown) and only insignificant alterations in the spike threshold of supralinear dendrites (figure 10). These simulations suggest that under physiological conditions, FS basket cells are highly likely to express two types of dendritic integration modes.

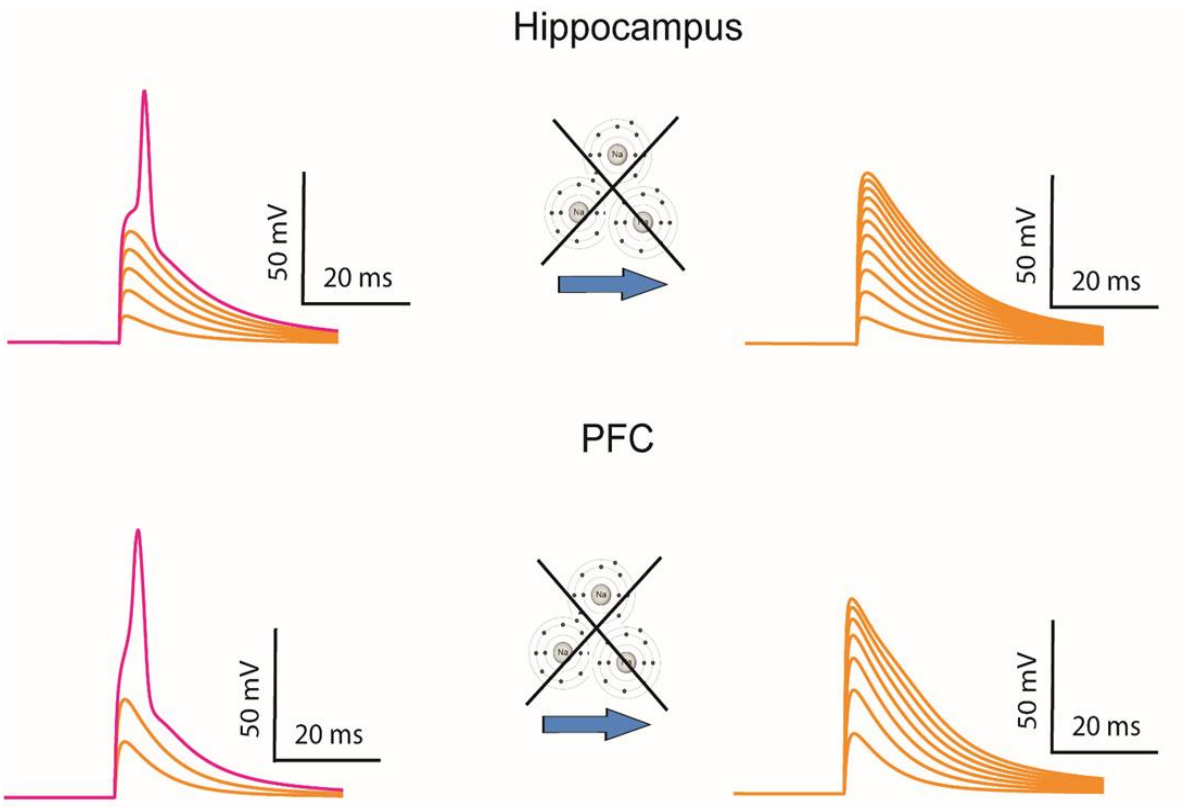

Figure 9: Block of sodium currents totally elliminates Supralinear mode, both in Hippocampus (up) and PFC (down).

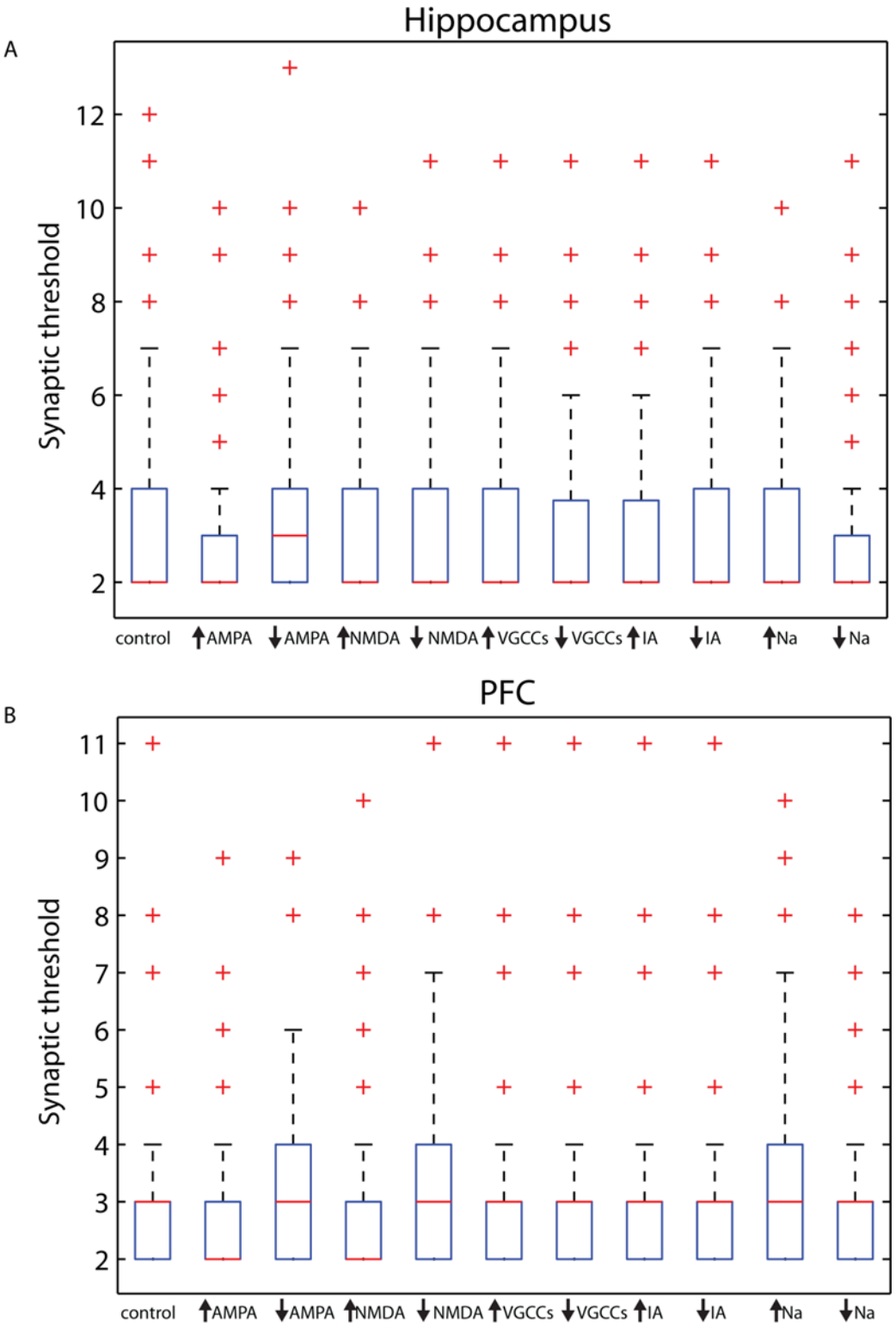

Figure 10:

Related to figure 2. Sensitivity analysis of biophysical dendritic mechanisms reveals minor changes in the synaptic threshold for spike generation in supralinear dendrites across Hippocampus (A) and PFC (B).

Table 6. Nonlinearity distributions		
Cell ID	Number of supralinear dendrites	Number of Sublinear dendrites
Hipp 1	95	67
Hipp 2	13	38
Hipp 3	10	41
Hipp 4	89	98
Hipp 5	27	32
PFC 1	36	7
PFC 2	48	5
PFC 3	43	14

Table 6: Number of supralinear and sublinear dendrites per cell.

3.3 Morphological determinants of dendritic integration modes.

Morphological features of dendrites were previously shown to influence synaptic integration profiles[61]. We thus investigated whether specific anatomical features correlate with the expression of each integration mode. We found that the mean dendritic diameter was highly statistically different (p-value=4.1966e-54) among sub- (thinner) and supra-linear (thicker) dendrites in the hippocampus (figure 11C) while in the PFC the dendritic length was a better determinant of sub- (shorter) vs. supra-linearity (longer) (p-value=7.6543e-05) (figure 11B). Length was less significant in the hippocampus (p-value=0.0064) (figure 11A) while diameter was not different among sub- and supralinear dendrites in the PFC (p-value=0.2454) (figure 11D). Dendritic volume considers both of the above features and serves as a robust morphological determinant for all dendrites in both areas (p-value=1.8433e-09), (figure 11E). These findings predict that morphology plays a crucial role in the spiking abilities of FS basket cell dendrites (figure 11F).

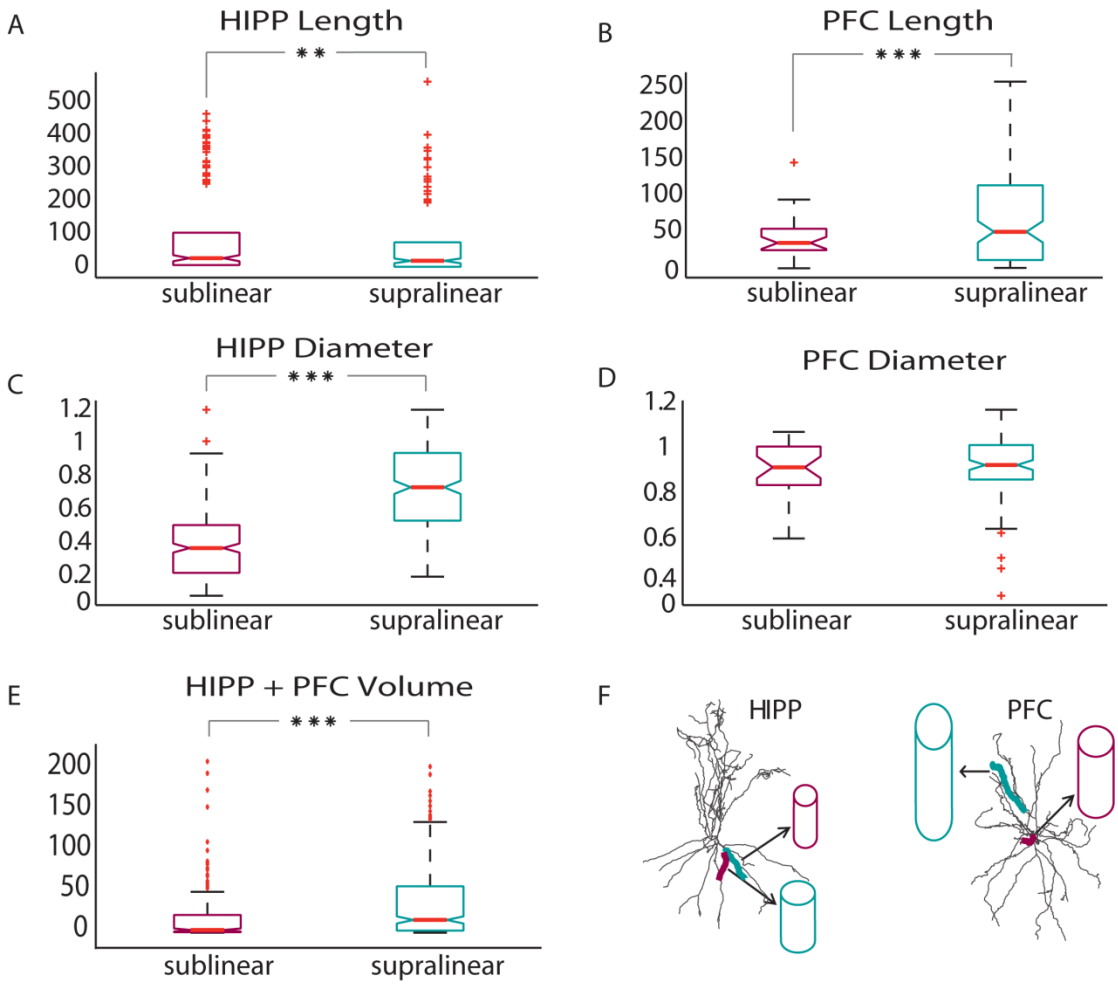

Figure 11: Morphological determinants of dendritic integration modes. A-B: Total length (µm) distributions of supralinear vs. sublinear dendrites in the hippocampus (A) and the PFC (B). Statistically significant differences are observed for both sub- and supra-linear models, in both areas. Significance is higher in PFC cells (p-value=7.6543e-05, 130 dendrites analyzed) compared to Hippocampal (p-value=0.0064, 507 dendrites analyzed) FS basket cells. C-D: Same as in A-B, for mean dendritic diameter (µm). Statistically significant differences are observed in Hippocampal (p-value=4.1966e-54, 507 dendrites analyzed) but not in PFC FS basket cells (p-value=0.2454, 130 dendrites analyzed). E. Dendritic Volume (μm^3) is a common discriminating characteristic among supralinear (larger) and sublinear dendrites, for both areas (p-value= p-value=1.8433e-09, 637 dendrites analyzed). F. Schematic illustration of distinctive morphological features for supralinear and sublinear dendrites in Hippocampus (left) and PFC (right).

3.4 Effect of bimodal dendritic integration on neuronal firing

In light of a bimodal dendritic integration in the modeled FS basket cells, the natural question that arises concerns the functional implications of such a property. To answer this question, we simulated a large variety of different spatial patterns of synaptic activation and assessed their effect on neuronal output. Specifically, we generated over 10,000 synaptic stimulus patterns, which comprised of 0 to 60 excitatory synapses (activated with random Poisson spike trains at 50 Hz) distributed within a few, strongly activated branches (clustered) or randomly distributed within the entire dendritic tree (dispersed).

Several stimulation protocols were devised, in which different numbers of synapses were activated in various locations within the dendritic tree (see Methods). Dendrites were selected at random and inputs were distributed uniformly within selected dendrites. For the dispersed case, we allocated 5 or 10 synapses in randomly selected dendrites, one at a time, while for the clustered case we allocated 10 or 20 synapses within an increasing number of branches. In all cases, the number of activated synapses increased gradually up to a maximum of 60, as this number was sufficient to induce spiking at gamma frequencies (30-100 Hz). This process was repeated k times (k = number of dendrites in each cell) to ensure full coverage of the entire tree. As expected given the two modes of dendritic integration, the localization of activated inputs affected neuronal firing. For a given number of activated synapses, dispersed activation led to higher somatic firing rates than clustered activation, both in Hippocampal (p-value=2.0914e-21, figure 12A) as well as in PFC FS basket cells (p-value=0.0051, figure 12B). Interestingly, this finding is opposite to what has been reported for pyramidal neurons, in which synapse clustering increases firing rates[52].

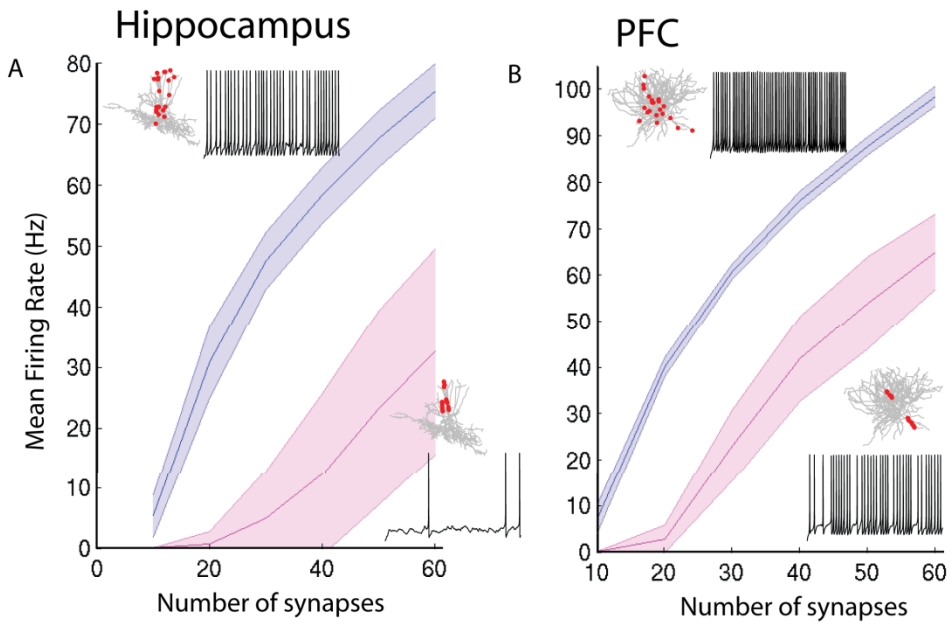

Figure 12: Effect of bimodal dendritic integration on neuronal firing. Firing rate responses (in Hz) from one Hippocampal (A) and one PFC (B) model cell, in response to stimulation of increasing numbers of synapses (10 to 60) that are either randomly distributed throughout the entire dendritic tree (blue) or clustered within a few dendritic branches (pink).) Synapses are stimulated with a 50 Hz Poisson spike train. Indicative somatic traces in response to stimulation of 30 synapses are shown for the four cases. Red dots represent the synaptic allocation motif.

3.5 FS basket cells as 2-layer artificial neural networks

The non-linear synaptic integration taking place within the dendrites of cortical[39] and CA1[37,40] pyramidal neurons was previously described as a sigmoidal transfer function[60]. Based on this reduction, a single pyramidal neuron was proposed to integrate its synaptic inputs like a 2-layer artificial neural network, where dendrites provide the hidden layer and the soma/axon the output layer[38]. To assess whether a similar mathematical formalization could be ascribed to our FS basket cell models, we constructed linear and non-linear artificial neural networks (as graphically illustrated in figure 13) and asked which of them can better capture the spike variance of the biophysical models.

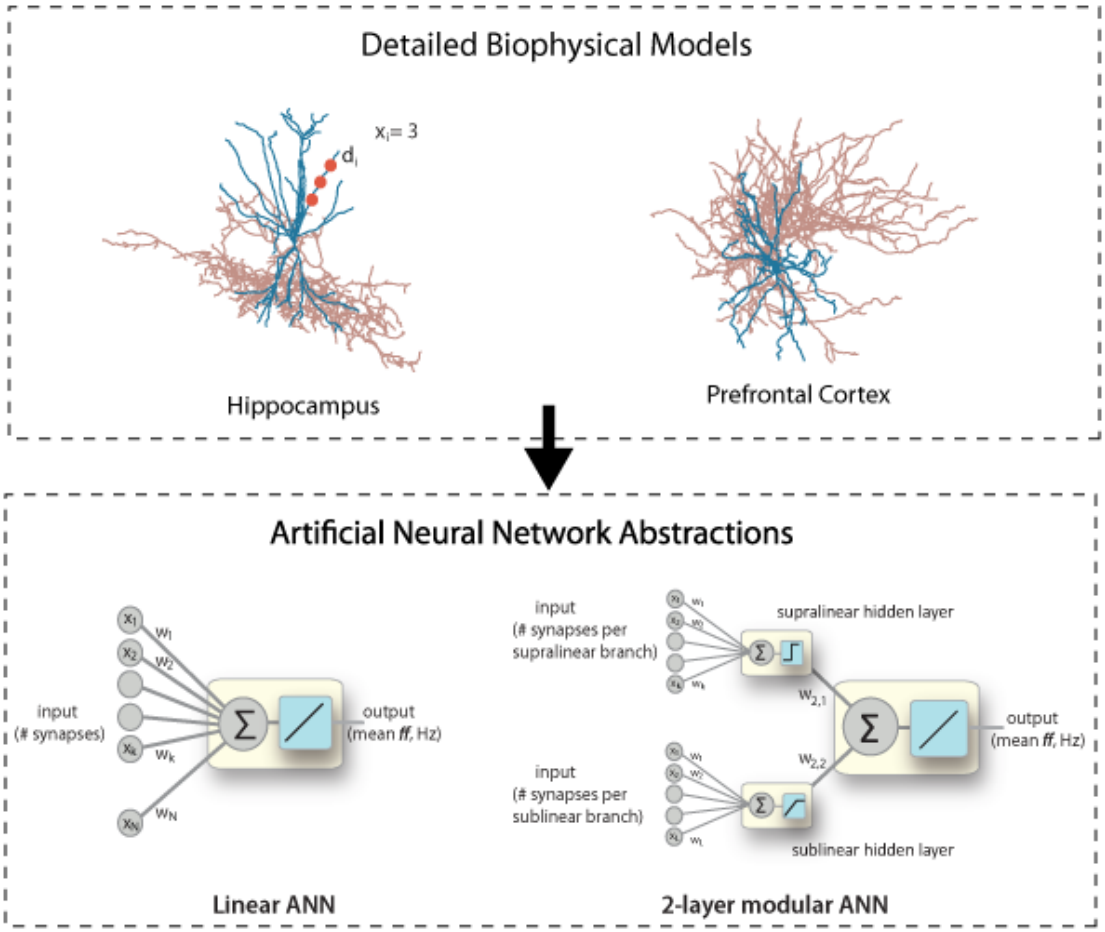

Figure 13: Reducing detailed compartmental models into mathematical abstractions. Two types of abstractions were used: a) a Linear ANN, in which the input (number of synapses) was linearly combined at the cell body and b) a 2-layer modular ANN, in which the input was fed into two parallel, separated hidden layers. The supralinear-layer was fed with the number of inputs landing onto supralinear branches while the sublinear layer was fed with the number of inputs landing onto sub-linear dendrites. Neurons in both hidden layers were equipped with nonlinear transfer functions, a step-sigmoid function in the supralinear layer and a saturating linear function in the sublinear layer. The somatic transfer functions of both ANNs were linear.

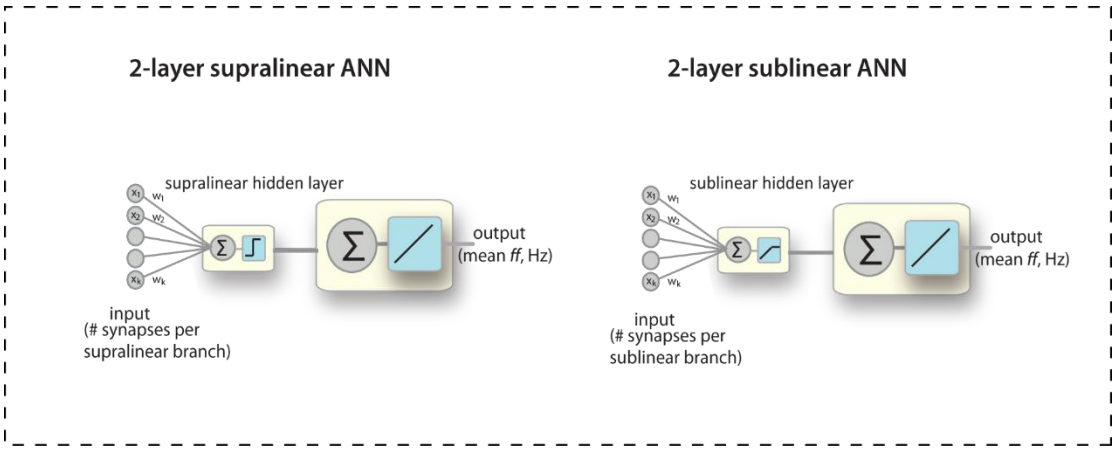

Figure 14:

Specifically, four types of feedforward, backpropagation Artificial Neural Networks (ANNs) were constructed (see Methods). In the *2-layer modular ANN*, supralinear and sublinear dendrites were simulated as 2 parallel hidden layers consisting of a step-sigmoidal and a saturating linear activation function, respectively[62] (figure 13). The total number of activated synapses allocated to supralinear and/or sublinear dendrites in the biophysical models was used as input to the respective hidden layers. The output layer represented the soma/axon of the biophysical model and consisted of a linear activation function. In the *linear ANN*, there was only a single hidden layer consisting of linear activation functions (figure 13). We also constructed two ANNs with the exact same architecture as the linear one, but with either a) a step-sigmoidal (*2-layer supralinear ANN*) or b) a saturating linear (*2-layer sublinear ANN*) activation function in the hidden layer neurons (figure 14). These ANNs represent FS basket cells with just one type of non-linear dendrites. The free parameters in all networks were identical (Table 5).

For a given hippocampal and a given mPFC biophysical model cell, the *linear* and *2-layer modular ANNs* were trained using the number of synapses to supra-/sublinear

dendrites as inputs to the respective hidden layers and the mean firing rate of the soma as target output. A randomly selected 70% of our synaptic activation data set (See Methods) was used to train the model and the rest to assess its generalization performance (15% Validation, 15% testing). Performance accuracy was estimated based on regression analysis between the ANN-generated firing rates and those produced by the biophysical models. The *2-layer modular ANN* reached an average performance accuracy of 96% and 95% (figure 15A, C) in predicting the spike rate variance in hippocampal and PFC models, respectively, while the *linear ANN* captured 85% and 75% of the spike rate variance, respectively (figure 15B, D). As expected, the *supralinear* and *sublinear ANNs* achieved intermediate accuracies for both hippocampal: 91%, 92% and PFC 90.8%, 92% models, indicating that both types of non-linear transfer functions are needed to capture the biophysical model variability (figure 16).

The relatively high performance of the *linear ANN* can be attributed to the wide range of activated synapses (2 to 60) which resulted in large differences in the somatic firing, irrespectively of synapse location, and can thus be captured by any linear model (also see[38]). To perform a fairer comparison, we also assessed the performance accuracy of *linear* and *2-layer modular ANNs* to the more challenging task of discriminating between input distributions corresponding to the exact same number of synapses. To do so, we subdivided the data into input categories corresponding to 20, 40 and 60 synapses, respectively. In this case, the *2-layer modular ANN* clearly outperformed the *linear ANN*, which failed to explain the variance produced by differences in input location (Table 7).

Taken together, this analysis suggests that a 2-layer artificial neural network that considers both types of dendritic non-linearities is a much better mathematical abstraction for FS basket cells than the currently assumed linear point neuron.

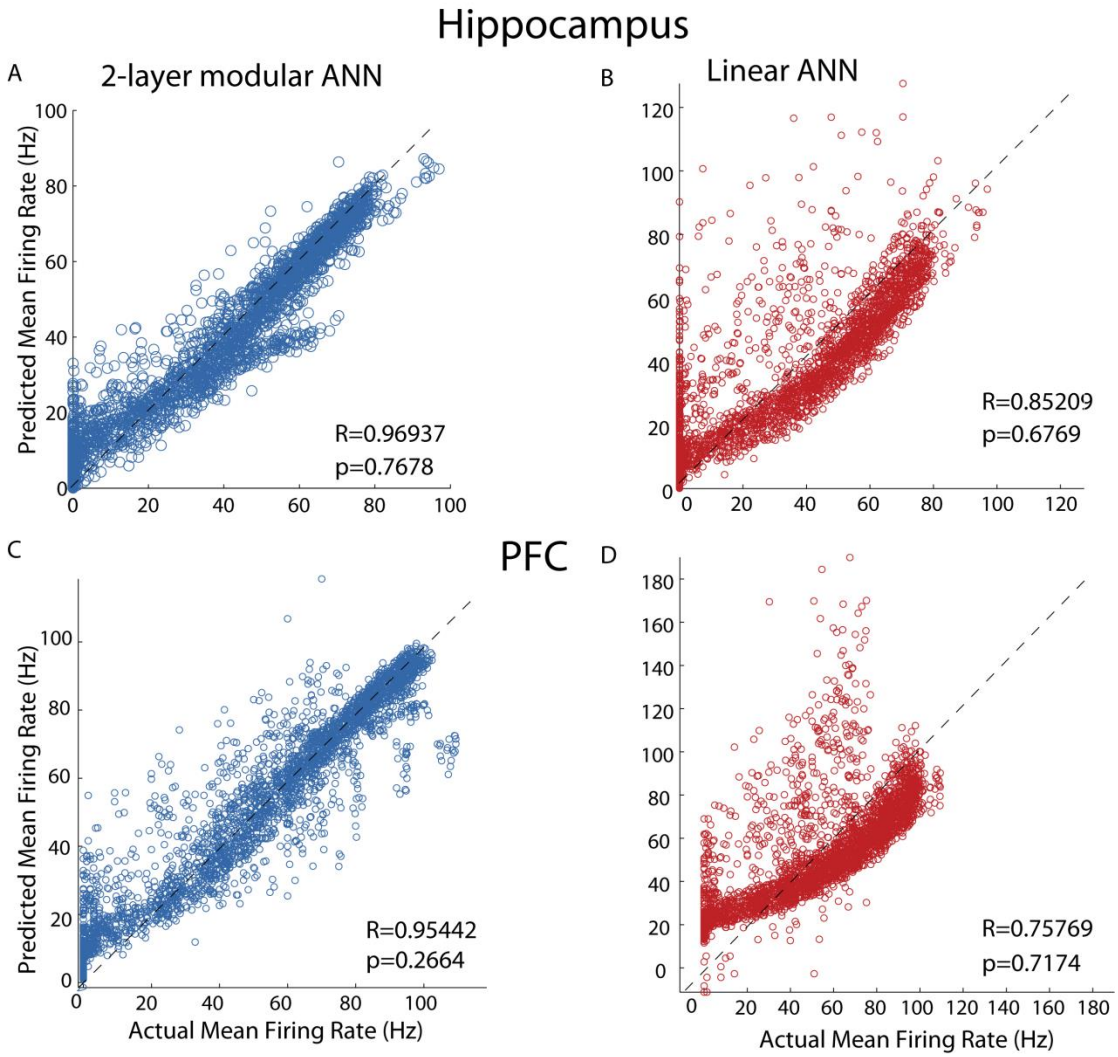

Figure 15: Challenging the point neuron dogma: FS basket cells as 2-stage nonlinear integrators. Linear regression analysis for 2-layer modular (A,C) and linear (B,D) ANNs for one indicative Hippocampal (top) and one indicative PFC (bottom) model cell. Actual Mean Firing Rates (Hz) correspond to the responses of the compartmental model when stimulating -with 50Hz Poisson spike trains- varying numbers of synapses (1 to 60), distributed in several ways (clustered or dispersed) within both sub- and supra-linear dendrites. Expected Mean Firing Rates (Hz) are those produced by the respective ANN abstraction when receiving the same input (number of stimulated synapses) in its respective sub-/supra- or linear input layer nodes.

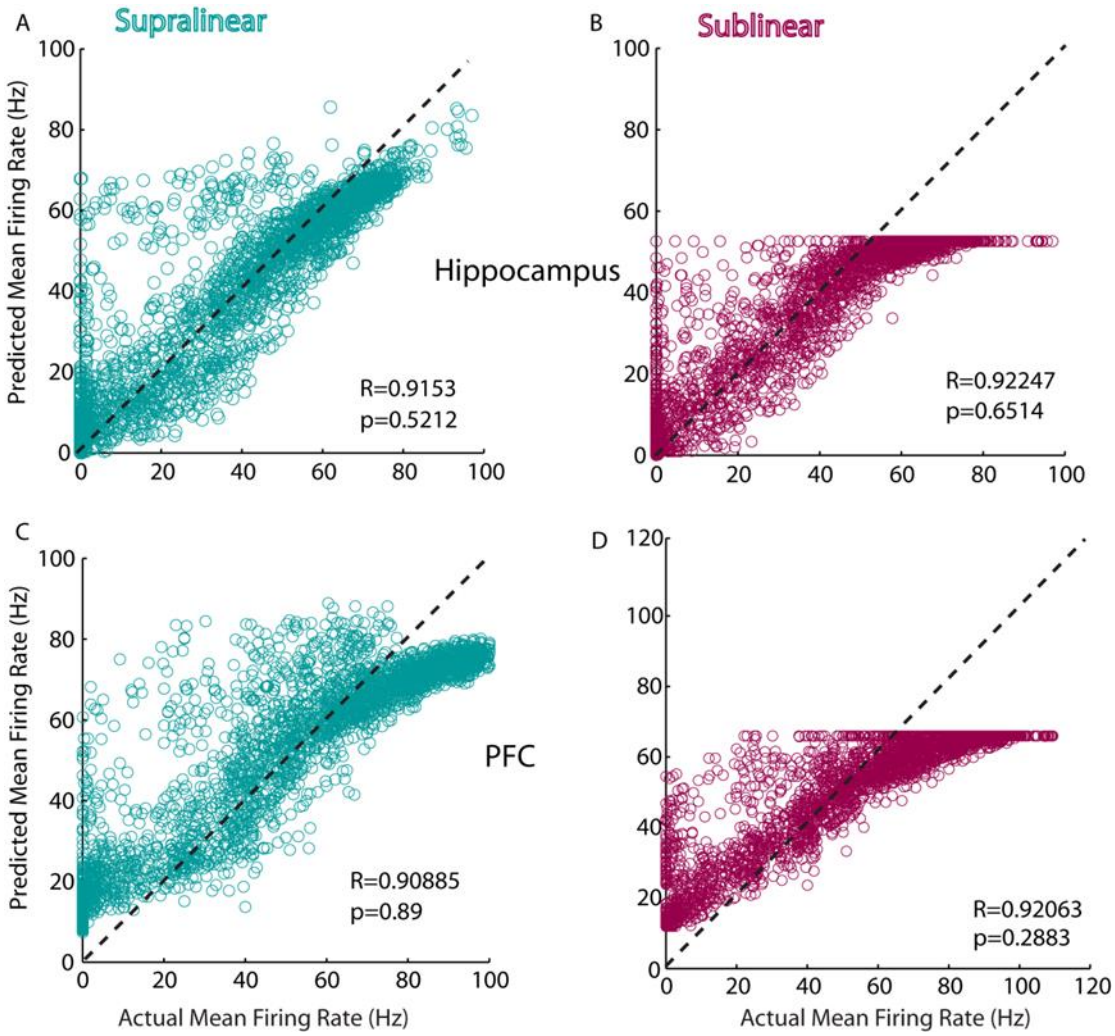

Figure 16. Related to figure 6. Challenging the point neuron dogma: FS basket cells as 2-stage nonlinear integrators. Linear regression analysis for one hidden layer supralinear (A,C) and one hidden layer sublinear (B,D) ANNs for one indicative Hippocampal (top) and one indicative PFC (bottom) model cell. Actual Mean Firing Rates (Hz) correspond to the responses of the compartmental model when stimulating -with 50Hz Poisson spike trains- varying numbers of synapses (1 to 60), distributed in several ways (clustered or dispersed) within both sub- and supra-linear dendrites. Expected Mean Firing Rates (Hz) are those produced by the respective ANN abstraction when receiving the same input (number of stimulated synapses) in its respective sub-/supra- or linear input layer nodes.

Table 7. ANN regression performance (R) for individual sets of synapses			
ANN type	*20 synapses*	*40 synapses*	*60 synapses*
2-layer modular ANN	**0.8994(HPC)/ 0.8750 (PFC)**	**0.9508 (HPC) / 0.8869 (PFC)**	**0.9406(HPC) /0.8399(PFC)**
Linear ANN	0.4862 (HPC) / 0.4867 (PFC)	0.6296 (HPC) / 0.5527 (PFC)	0.6801 (HPC) / 0.5136 (PFC)
2-layer supralinear ANN	0.6486 (HPC) / 0.7468 (PFC)	0.8172 (HPC) / 0.7995 (PFC)	0.8474 (HPC) /0.6633 (PFC)
2-layer sublinear ANN	0.7645 (HPC) / 0.8130 (PFC)	0.8816 (HPC) / 0.8487 (PFC)	0.8617 (HPC) /0.7674 (PFC)

Table 7: Comparison of ANN prediction accuracy (measured as the correlation coefficient, R) for all four ANN reductions, when tested on three sets of synaptic inputs consisting of 20, 40 or 60 activated synapses, respectively. Synapses were randomly distributed in various ways/locations in the biophysical model cells and resulting firing rates were used as target vectors for the ANNs. The 2-layer modular ANN is clearly superior to the Linear ANN when it comes to capturing location-induced firing-rate variability.

4 DISCUSSION

The role of dendrites in interneuron computations is a rapidly emerging and debatable subject[45]. Several recent reports present exciting findings according to which dendrites may serve as key players[7,17,47,48,63]. For example, sodium spikes and supralinear calcium accumulation have recently been reported in the dendrites of FS basket cells[7,45,64], yet the consensus still favors the linear point neuron dogma[11,45,65]. The present study provides new insight into this ongoing debate by systematically analyzing the dendritic integration mode of FS basket cells in two widely studied areas: the Hippocampus and the PFC. We predict that dendrites of both cortical and hippocampal FS basket cells operate in one of two modes of synaptic integration: supralinear or sublinear (figure 6). Supralinearity is due to the generation of dendritic sodium spikes, and can be facilitated –or prohibited as in sublinear dendrites- by the morphology (diameter, length, volume, (figure 11)) of dendrites. Moreover, we find that somatic output is influenced by the

spatial distribution of activated synapses, with dispersed stimulation inducing higher firing rates than clustered stimulation (figure 12). Due to these properties, a 2-layer Artificial Neural Network abstraction with both sub- and supra-linear hidden neurons captures the spiking profile of biophysical neurons with much higher accuracy compared to a linear ANN, analogous to a point neuron (figures 13,15). These findings suggest that the dendrites of FS basket cells in both the hippocampus and the cortex can support two types of non-linear computations and are the first to explicitly challenge the point neuron dogma.

4.1 Mediators of supralinear and sublinear dendritic integration in FS basket cells

A bimodal dendritic integration is predicted for all hippocampal and PFC morphologies analyzed. In all cases, supralinearity is due to the occurrence of dendritic sodium spikes. Several mechanisms can influence the generation of such dendritic spikes: ionic conductances (primarily of sodium currents but also potassium currents) and morphological features. In our models, biophysical mechanisms are constrained by existing experimental data and dendritic sodium conductances are kept to a minimum (10 times smaller than the soma[11]), so as to minimize the probability of non-physiological dendritic spiking. Sensitivity analysis further demonstrates that results are robust to physiological variations in a wide range of dendritic conductances. These findings strongly suggest that dendritic spiking in certain dendrites of FS basket cells are highly likely to occur under physiological conditions, in line with recent experimental reports[7]. Apart from sodium currents as a universal enabling mechanism, we find a key role of morphology in gating local dendritic spikes. A combination of dendritic length and mean diameter, or otherwise the dendritic volume, is statistically different between sub- (smaller) and supralinear (larger) dendrites across all morphologies tested. These results are in line with other studies reporting a similar effect of morphology on the ability of dendrites to generate local spikes[66].

4.2 Functional coexistence of sub- and supra-linear dendrites within FS basket cells

Our simulations predict the co-existence of both sublinear and supralinear dendrites in all simulated FS basket cells (figures 6, 7, 8). Similar bimodal dendritic integration has been reported in hippocampal CA1 pyramidal neurons[37,40] and predicted in PFC pyramidal neurons[67]. However, the functional consequences of this coexistence in interneurons requires further investigation.

The existence of sublinear dendritic branches supports the idea of inhibitory neurons acting as coincidence detectors by aggregating spatially disperse and nearly synchronous synaptic inputs[11]. Moreover, sub-linear dendrites can compute complex non-linear functions similar to those computed by sigmoidal dendrites[60], thus substantially extending the processing capacity of these neurons compared to a linear integrator. Why have two types of nonlinearity then?

One possibility is to enable the detection of few but highly correlated inputs: via spatial clustering onto supralinear dendrites these inputs would reliably induce dendritic spikes capable of overcoming the dampening effects of inhibitory conductances, thus generating strong somatic responses. Another possibility entails increases in flexibility through the ability to (a) engage intrinsic plasticity mechanisms (e.g. regulation of potassium channels) and/or (b) to dynamically tune the neuronal operation mode from generic (sublinear domination) to specific (supralinear domination), depending on the behavioral state. As dendrites of FS basket cells often cross layers and receive input from different afferent pathways[68], another possibility is that feedback vs. feedforward pathways target dendrites with distinct modes of integration. These scenarios can be tested in future studies engaging network models and/or experimental probing.

4.3 Not that Simple: FS basket cells as 2-layer modular ANNs

Artificial Neural Network analysis demonstrates that a FS basket cell is better described by a 2-stage abstraction, which takes into account both modes of dendritic integration. This work, along the lines of the 2-stage model proposed for pyramidal neurons[38], strongly challenges the prevailing point neuron dogma. The 2-stage abstraction is supported by experimental reports of dendritic sodium spikes and supralinear calcium accumulations[7] while it also explains sublinear dendritic integration[11,17,32,69], providing a unifying framework for interneuron processing.

Possible limitations of our work include the imprecise modeling of ionic and synaptic mechanisms given the shortage of sufficient information for FS basket cells. This limitation is counteracted by the sensitivity analysis of the mechanisms that mostly influence our findings and their consistency across several cortical and hippocampal morphologies. Another limitation is the lack of inhibitory inputs (except from the autaptic GABAa current that is incorporated in all models) and gap junctions on our model cells. Inhibitory inputs consist of just 6% of all incoming contacts in Fast Spiking interneurons[11,50,70]. Thus, our results are unlikely to be affected by inhibitory inputs. FS basket cells in the hippocampus and the neocortex are highly interconnected by gap junctions[11], that can speed the EPSP time course, boost the efficacy of distal inputs and increase the average action potential frequency after repetitive synaptic activation.[11] All of these effects would contribute to stronger responses but unless gap junctions are spatially specific to certain branches and not others, they are unlikely to influence the non-linear integration modes of dendrites.

5 Conclusion

This work provides a novel view of dendritic integration in FS basket cells, that extends in hippocampal and cortical areas[71]. To our knowledge, we are the first to suggest a new reductionist model for interneuron processing, in which dendrites play a crucial role. Experimental validation of this new model is likely to change the way we think about interneuron processing, attribute new and exciting roles to FS basket cells and open new avenues for understanding interneuron contributions to brain function.

6 References

1. Squire, L. R., Stark, C. E. L. & Clark, R. E. THE MEDIAL TEMPORAL LOBE. *Annu. Rev. Neurosci.* **27,** 279–306 (2004).

2. O'Keefe, J., Burgess, N., Donnett, J. G., Jeffery, K. J. & Maguire, E. A. Place cells, navigational accuracy, and the human hippocampus. *Philos. Trans. R. Soc. B Biol. Sci.* **353,** 1333–1340 (1998).

3. Amaral, D. G. & Lavenex, P. in *The hippocampus book* (eds. Andersen, P., Morris, R., Amaral, D. G., Bliss, T. & O'Keefe, J.) 37–100 (Oxford University Press, Inc., 2007).

4. Kolb, B. *et al.* Experience and the developing prefrontal cortex. *Proc. Natl. Acad. Sci.* **109,** 17186–17193 (2012).

5. Frankland, P. W. & Bontempi, B. The organization of recent and remote memories. *Nat. Rev. Neurosci.* **6,** 119–130 (2005).

6. Buzsáki, G., Geisler, C., Henze, D. A. & Wang, X.-J. Interneuron Diversity series: Circuit complexity and axon wiring economy of cortical interneurons. *Trends Neurosci.* **27,** 186–193 (2004).

7. Chiovini, B. *et al.* Marti. *Neuron* **82,** 908–924 (2014).

8. Freund, T. F. Interneuron Diversity series: Rhythm and mood in perisomatic inhibition. *Trends in Neurosciences* (2003). doi:10.1016/S0166-2236(03)00227-3

9. Kann, O. The interneuron energy hypothesis: Implications for brain disease. *Neurobiol. Dis.* **90,** 75–85 (2016).

10. Tremblay, R., Lee, S. & Rudy, B. GABAergic Interneurons in the Neocortex: From Cellular Properties to Circuits. *Neuron* **91,** 260–292 (2016).

11. Hu, H., Gan, J. & Jonas, P. Interneurons. Fast-spiking, parvalbumin^{+} GABAergic interneurons: from cellular design to microcircuit function. *Science* **345,** 1255263 (2014).

12. Klausberger, T. & Somogyi, P. Neuronal diversity and temporal dynamics: the unity of hippocampal circuit operations. *Science* **321,** 53–7 (2008).

13. Van Aerde, K. I. *et al.* Flexible spike timing of layer 5 neurons during dynamic beta oscillation shifts in rat prefrontal cortex. *J. Physiol.* **587,** 5177–5196 (2009).

14. Averkin, R. G., Szemenyei, V., Bordé, S. & Tamás, G. Identified Cellular Correlates of Neocortical Ripple and High-Gamma Oscillations during Spindles of Natural Sleep. *Neuron* (2016). doi:10.1016/j.neuron.2016.09.032

15. Somogyi, P. & Klausberger, T. Defined types of cortical interneurone structure space and spike timing in the hippocampus. *J. Physiol.* **562,** 9–26 (2005).

16. Tremblay, R., Lee, S. & Rudy, B. GABAergic Interneurons in the Neocortex: From Cellular Properties to Circuits. *Neuron* **91,** 260–292 (2016).

17. Abrahamsson, T., Cathala, L., Matsui, K., Shigemoto, R. & DiGregorio, D. A. Thin Dendrites of Cerebellar Interneurons Confer Sublinear Synaptic Integration and a Gradient of Short-Term Plasticity. *Neuron* **73,** 1159–1172 (2012).

18. Nörenberg, A., Hu, H., Vida, I., Bartos, M. & Jonas, P. Distinct nonuniform cable properties optimize rapid and efficient activation of fast-spiking GABAergic interneurons. *Proc. Natl. Acad. Sci. U. S. A.* **107,** 894–9 (2010).

19. Freund, T. F. & Katona, I. Perisomatic Inhibition. *Neuron* (2007). doi:10.1016/j.neuron.2007.09.012

20. Lee, S.-H. *et al.* Parvalbumin-Positive Basket Cells Differentiate among Hippocampal Pyramidal Cells. *Neuron* **82,** 1129–1144 (2014).

21. Povysheva, N. V *et al.* Parvalbumin-positive basket interneurons in monkey and rat prefrontal cortex. *J. Neurophysiol.* **100,** 2348–60 (2008).

22. Hioki, H. *et al.* Cell type-specific inhibitory inputs to dendritic and somatic compartments of parvalbumin-expressing neocortical interneuron. *J. Neurosci.* **33,** 544–55 (2013).

23. Hainmüller, T., Krieglstein, K., Kulik, A. & Bartos, M. Joint CP-AMPA and group I mGlu receptor activation is required for synaptic plasticity in dentate gyrus fast-spiking interneurons. *Proc. Natl. Acad. Sci. U. S. A.* **111,** 13211–6 (2014).

24. Geiger, J. R. P. *et al.* Relative abundance of subunit mRNAs determines gating and Ca2+ permeability of AMPA receptors in principal neurons and interneurons in rat CNS. *Neuron* **15,** 193–204 (1995).

25. Bacci, A., Rudolph, U., Huguenard, J. R. & Prince, D. A. Cellular/Molecular Major Differences in Inhibitory Synaptic Transmission onto Two Neocortical Interneuron Subclasses.

26. Goldberg, E. M. *et al.* K+ channels at the axon initial segment dampen near-threshold excitability of neocortical fast-spiking GABAergic interneurons. *Neuron* **58,** 387–400 (2008).

27. Kim, D. *et al.* Distinct Roles of Parvalbumin- and Somatostatin-Expressing Interneurons in Working Memory. *Neuron* (2016). doi:10.1016/j.neuron.2016.09.023

28. Kim, H., Ährlund-Richter, S., Wang, X., Deisseroth, K. & Carlén, M. Prefrontal Parvalbumin Neurons in Control of Attention. *Cell* **164,** 208–218 (2016).

29. Povysheva, N. V, Zaitsev, A. V, Gonzalez-Burgos, G. & Lewis, D. A. Electrophysiological heterogeneity of fast-spiking interneurons: chandelier versus basket cells. *PLoS One* **8,** e70553 (2013).

30. Rudy, B. & McBain, C. J. Kv3 channels: voltage-gated K+ channels designed for high-frequency repetitive firing. *Trends Neurosci.* **24,** 517–526 (2001).

31. Martina, M. & Jonas, P. Functional differences in Na + channel gating between fast-spiking interneurones and principal neurones of rat hippocampus. *J.*

Physiol. **505,** 593–603 (1997).

32. Hu, H., Martina, M. & Jonas, P. Dendritic Mechanisms Underlying Rapid Synaptic Activation of Fast-Spiking Hippocampal Interneurons. *Science (80-.).* **327,** 52–58 (2010).

33. Silver, R. A. Neuronal arithmetic. *Nat. Rev. Neurosci.* **11,** 474–489 (2010).

34. Polsky, A., Mel, B. W. & Schiller, J. Computational subunits in thin dendrites of pyramidal cells. *Nat. Neurosci.* **7,** 621–7 (2004).

35. Papoutsi, A., Kastellakis, G., Psarrou, M., Anastasakis, S. & Poirazi, P. Coding and decoding with dendrites. *J. Physiol.* **108,** 18–27 (2014).

36. Häusser, M. & Mel, B. Dendrites: bug or feature? *Curr. Opin. Neurobiol.* **13,** 372–383 (2003).

37. Poirazi, P., Brannon, T. & Mel, B. W. Arithmetic of Subthreshold Synaptic Summation in a Model CA1 Pyramidal Cell. *Neuron* **37,** 977–987 (2003).

38. Poirazi, P., Brannon, T. & Mel, B. W. Pyramidal Neuron as Two-Layered Neural Network. *Neuron* **37,** 989–999 (2003).

39. Larkum, M. E., Nevian, T., Sandler, M., Polsky, A. & Schiller, J. Synaptic Integration in Tuft Dendrites of Layer 5 Pyramidal Neurons: A New Unifying Principle. *Science (80-.).* **325,** (2009).

40. Losonczy, A. & Magee, J. C. Integrative Properties of Radial Oblique Dendrites in Hippocampal CA1 Pyramidal Neurons. *Neuron* **50,** 291–307 (2006).

41. Branco, T. & Häusser, M. *Synaptic Integration Gradients in Single Cortical Pyramidal Cell Dendrites*. *Neuron* **69,** (2011).

42. Spruston, N. Pyramidal neurons: dendritic structure and synaptic integration. *Nat. Rev. Neurosci.* **9,** 206–221 (2008).

43. Cazé, R. D., Jarvis, S., Foust, A. J. & Schultz, S. R. *Dendrites enable a robust mechanism for neuronal stimulus selectivity*. *bioRxiv* (Cold Spring Harbor Labs Journals, 2015). doi:10.1101/023200

44. Stuart, G. J. & Spruston, N. Dendritic integration: 60 years of progress. *Nat. Neurosci.* **18,** 1713–1721 (2015).

45. Hu, H. & Vervaeke, K. Synaptic Integration in Cortical Inhibitory Neuron Dendrites. *Neuroscience* **368,** 115–131 (2018).

46. Goldberg, J. H., Tamas, G. & Yuste, R. Ca2+ imaging of mouse neocortical interneurone dendrites: Ia-type K+ channels control action potential backpropagation. *J. Physiol.* **551,** 49–65 (2003).

47. Tran-Van-Minh, A., Abrahamsson, T., Cathala, L. & DiGregorio, D. A. Differential Dendritic Integration of Synaptic Potentials and Calcium in Cerebellar Interneurons. *Neuron* **91,** 837–850 (2016).

48. Katona, G. *et al.* Roller Coaster Scanning reveals spontaneous triggering of dendritic spikes in CA1 interneurons. *Proc. Natl. Acad. Sci. U. S. A.* **108,**

2148–2153 (2011).

49. Branco and Hausser, M, T. The single dendritic branch as a fundamental functional unit in the nervous system. *Curr. Opin. Neurobiol.* **20,** 494–502 (2010).

50. Tukker, J. J. *et al.* Distinct Dendritic Arborization and In Vivo Firing Patterns of Parvalbumin-Expressing Basket Cells in the Hippocampal Area CA3. *J. Neurosci.* **33,** (2013).

51. Rotaru, D. C., Yoshino, H., Lewis, D. A., Ermentrout, G. B. & Gonzalez-Burgos, G. Glutamate Receptor Subtypes Mediating Synaptic Activation of Prefrontal Cortex Neurons: Relevance for Schizophrenia. *J. Neurosci.* **31,** 142–156 (2011).

52. Kastellakis, G., Cai, D. J., Mednick, S. C., Silva, A. J. & Poirazi, P. Synaptic clustering within dendrites: An emerging theory of memory formation. *Prog. Neurobiol.* **126,** 19–35 (2015).

53. Hines, M. L. & Carnevale, N. T. The NEURON Simulation Environment. *Neural Comput.* **9,** 1179–1209 (1997).

54. Emri, Z., Antal, K., Gulyás, A. I., Megías, M. & Freund, T. F. Electrotonic profile and passive propagation of synaptic potentials in three subpopulations of hippocampal CA1 interneurons. *Neuroscience* **104,** 1013–1026 (2001).

55. Konstantoudaki, X., Papoutsi, A., Chalkiadaki, K., Poirazi, P. & Sidiropoulou, K. Modulatory effects of inhibition on persistent activity in a cortical microcircuit model. *Front. Neural Circuits* **8,** (2014).

56. Goldberg, J. H., Yuste, R. & Tamas, G. Ca2+ imaging of mouse neocortical interneurone dendrites: contribution of Ca2+-permeable AMPA and NMDA receptors to subthreshold Ca2+dynamics. *J. Physiol.* **551,** 67–78 (2003).

57. Goldberg, J. H. & Yuste, R. Space matters: Local and global dendritic Ca2+ compartmentalization in cortical interneurons. *Trends Neurosci.* **28,** 158–167 (2005).

58. Wang, H.-X. & Gao, W.-J. Cell type-specific development of NMDA receptors in the interneurons of rat prefrontal cortex. *Neuropsychopharmacology* **34,** 2028–40 (2009).

59. Connelly, W. M. & Lees, G. Modulation and function of the autaptic connections of layer V fast spiking interneurons in the rat neocortex. *J. Physiol.* **588,** 2047–63 (2010).

60. Cazé, R. D., Humphries, M., Gutkin, B., Tank, D. & DiGregorio, D. Passive Dendrites Enable Single Neurons to Compute Linearly Non-separable Functions. *PLoS Comput. Biol.* **9,** e1002867 (2013).

61. Tran-Van-Minh, A. *et al.* Contribution of sublinear and supralinear dendritic integration to neuronal computations. *Front. Cell. Neurosci.* **9,** 67 (2015).

62. Cazé, R. D., Humphries, M. & Gutkin, B. Passive dendrites enable single neurons to compute linearly non-separable functions. *PLoS Comput. Biol.* **9,** e1002867 (2013).

63. Topolnik, L. Dendritic calcium mechanisms and long-term potentiation in cortical inhibitory interneurons. *Eur. J. Neurosci.* **35,** 496–506 (2012).

64. Camire, O. & Topolnik, L. Dendritic Calcium Nonlinearities Switch the Direction of Synaptic Plasticity in Fast-Spiking Interneurons. *J. Neurosci.* **34,** 3864–3877 (2014).

65. Hu, H., Martina, M. & Jonas, P. Dendritic Mechanisms Underlying Rapid Synaptic Activation of Fast-Spiking Hippocampal Interneurons. *Science (80-.).* **327,** 52–58 (2010).

66. Tran-Van-Minh, A. *et al.* Contribution of sublinear and supralinear dendritic integration to neuronal computations. *Front. Cell. Neurosci.* **9,** 67 (2015).

67. Larkum, M. E., Nevian, T., Sandler, M., Polsky, A. & Schiller, J. Synaptic Integration in Tuft Dendrites of Layer 5 Pyramidal Neurons: A New Unifying Principle. *Science (80-.).* **325,** (2009).

68. Kohus, Z. *et al.* Properties and dynamics of inhibitory synaptic communication within the CA3 microcircuits of pyramidal cells and interneurons expressing parvalbumin or cholecystokinin. *J. Physiol.* **594,** 3745–74 (2016).

69. Martina, M. Distal Initiation and Active Propagation of Action Potentials in Interneuron Dendrites. *Science (80-.).* **287,** 295–300 (2000).

70. Gulyás, A. I., Megías, M., Emri, Z. & Freund, T. F. Total Number and Ratio of Excitatory and Inhibitory Synapses Converging onto Single Interneurons of Different Types in the CA1 Area of the Rat Hippocampus. *J. Neurosci.* **19,** (1999).

71. Kastellakis, G., Silva, A. J. & Poirazi, P. Linking Memories across Time via Neuronal and Dendritic Overlaps in Model Neurons with Active Dendrites. *Cell Rep.* **17,** 1491–1504 (2016).